Energy-Aware Grid Based Coverage Path Planning for UAVs

Alia Ghaddar
Department of Computer Science
International University of Beirut, BIU/LIU
Beirut, Lebanon
email: alia.ghaddar@liu.edu.lb

Ahmad Merei
Department of Computer Science
International University of Beirut, BIU/LIU
Beirut, Lebanon
email: 41430485@students.liu.edu.lb

***Abstract*—The usage of Unmanned Aerial Vehicles (UAVs) for different tasks has rapidly increased in recent years. An Unmanned Aerial Vehicle is an unpiloted aircraft that operates by remote control or onboard computers. This technology has become promising in providing new opportunities in many fields, such as smart agriculture, photogrammetry, remote sensing, wireless coverage, rescuing and many others. Controlling the mobility of an Unmanned Aerial Vehicle while monitoring geographical zones is one of the most important problems. In this context, managing the flight route by finding an optimal path that fully covers the Area of Interest with minimum energy consumption is one of the main challenges. In this work, we propose an algorithm to scan an area that reduces completion-time and energy consumption. It also ensures a complete coverage of the area. We consider an Area of Interest without obstacles and non-flying zones.**

Keywords*—*Unmanned Aerial Vehicles; Coverage Path Planning; Energy-Aware Trajectories; Remote Sensings; Cellular Decomposition.

I. Introduction

The rapid technology dissemination and advances in the control field and Micro Electro Mechanical Systems (MEMS) gave rise to a new chain of developments on mini UAVs. The usage of UAVs or drones in remote sensing scenarios has grown fast in the last years. Many application domains address terrain coverage, such as surveillance [1], smart farming [2], photogrammetry [3], disaster management [4–7], civil security, wildfire tracking [8–11] and many others [3][12][13]. Coverage Path Planning (CPP) is basically finding the route that covers every point of a certain Area of Interest (AoI). A main requirement in CPP is to reduce the completion-time of the overall mission and, at the same time, to ensure a complete coverage of the area. The key elements in the scanning mission are the drones types and the trajectory plan.

A. Drone Type and Application domains

UAVs can be divided into three main types: Rotary Wing, Fixed Wing and Hybrid [14–16]. They have different features, sizes and specifications like footprint, weight, power support (gas, electric, nitro, solar, etc.).

Rotory drones, also known as rotary-wings drones, allow vertical take-off and landing. They may hover over a fixed location to produce continuous cellular coverage. This type of aerial platform can also be classified into single-rotor (helicopter) and multi-rotor (quadcopter and hexacopter). Quadcopters are inexpensive and have good maneuverability. They are widely applied in surveillance missions, such as in confined spaces and close-range inspection tasks, marine settings and terrestrial areas with steep terrain, or extensive vegetation cover [14][17].

Fixed wing drones are comparatively weighty, as they need significant battery power. However, they have the advantage of carrying higher payloads. Furthermore, they are suitable to be deployed in a large area because of their high durability and long flight time duration. However, they cannot focus on the same scene for a long period of time due to their high speed. They cannot stop or slow down the speed during the mission. Thus, fixed wing drones cannot be used as remote flying camera controllers as they need high speed sensors to survey [18].

Hybrid drones can switch their flight/operation mode: in one mode they are ready to float, similar to helicopters, and in the alternative mode, they fly, similar to fixed wing drones.

UAVs are used in various fields ranging from the military, humanitarian relief, disaster management to agriculture. Below we present a few typical examples [19–21]:

- Rescue and search: Drones can be used in emergency cases for rescue and search. They can overcome the difficulty of crossing areas that humans cannot reach, bridging isolated areas and enhancing wireless coverage.
- Smart policing: Most of the cities police or private agencies use drones to keep an eye on the crowd during any event. It also provides detailed documentation of a crime and accident scenes.
- Smart transportation and monitoring systems: New UAV application areas are enabled by Internet of Things (IoT). Drone mapping capabilities are helping set the foundation for the future. They offer many services and opportunities that can benefit smart cities applications (medical [22], package delivery, traffic monitoring and firefighting) [23]. Commercial applications are focused on delivering products via new type of smart transportation systems from depots to homes of end-users.
- Smart agriculture: Monitoring the growing process of plants can benefit from the use of drones. Data collected from UAVs can be used for the analysis of soils and drainage. It can also be used for the crop

 ISBN: 978-1-61208-744-3

health assessment. The use of drones gives farmers a richer picture of their fields.
- Entertainment and Media: Advertising, entertainment, aerial photography, shows and special effects [24].
- Security: Monitoring lines and sites, proactive response.
- Telecommunication: Tower maintenance, signal broadcasting.

B. Motivation

The energy constraints and flight limitations of UAVs have attracted significant attention from researches as they directly impact the network performance in Coverage Path Planning missions [25–28]. On-board energy in UAV are consumed for powering the movements of the drone (hovering, horizontal and vertical motions). However, increasing battery size is not an alternative key solution as the energy consumption increases when the drone carries extra payload and has more weight [29][30]. Moreover, additional energy could be consumed in the air in the presence of winds [31–33].

Two main performance metrics mainly reflects energy consumption and completion-time. These metrics are path length (or the traveled distance) [12][34] and the number of turns [18][29]. The number of turns during a mission impacts the time needed to accomplish the entire path. In [35], authors rely on these metrics to find the optimal path. These metrics are compared and investigated in [36]. Studies show that, for UAVs, a path with less turns is more efficient in terms of route length, duration and energy. Lowering the number of turns leads to a lower delay in completion-time and thus to a shorter path. Consequently, lower energy consumption is resulted.

In our work, we consider having one rotary wing drone. We aim to cover an Area of Interest without obstacles and non-flying zones. The main challenges in our work are as follows: achieving minimum completion-time, minimum number of turns, lowering the energy consumption, and having a shortest mission path to cover the whole area. The method described in this paper makes use of grid partitioning to reach its goal.

The rest of this paper is organized as follows. The related works are presented in Section II. In Section III, we present our contribution. The computational experiments and results are discussed in Section IV. Section V concludes our paper.

II. Related Works

The Internet of Flying Robots (IoFR) is a sub-concept of the Internet of Things (IoT) [37] and Internet of Robotic Things [38]. The Rlying Robots (FRs) may refer to drones, UAVs, or airships in different applications [39]. CPP is classified as subtopic of the path planning in robotics. Its objective is to cover a free space in an environment and obtaining a low cost path with minimum overlapping [40]. Various approaches have been proposed to compute a low cost coverage path [41–43] such as mirror mapping method [44], in-field obstacles classification [45], context-aware UAV mobility [46]. Among the different decomposition-based coverage methods that are used for coverage applications, we mention Classical exact cellular decomposition [47], Boustrophedon decomposition [48] and trapezoidal decomposition [49], landmark based topological coverage [50] and grid-based methods [51]. Several research studies focus on the Coverage Path Planning from different perspectives. They propose trajectory solutions with different scenarios taking into consideration different factors: area shape, status of the plan (Online/offline), number of drones, completion-time, energy consumption.

A. Area shape and Plan status

The area shape plays a role in defining the trajectory method for coverage. An AoI could have a regular shape [55][56][60] or an irregular shape [17]. A review of existing approaches resulted in works that explore rectangular areas. Others assume convex polygonal environments with different type of sensors mounted on the UAV (visual sensors, thermal sensors, etc) [36][52][65]. Information about the environment is either available offline or online. Several approaches consider online path plan mainly used to cover mobile sensors in real-time or to modify path depending on sudden changes in the surrounding atmosphere [66]. The basic approach for Offline CPP algorithms is the area decomposition, determining the visiting sequence of the sub regions, and covering decomposed regions to obtain a complete coverage path [43][67][68].

B. Coverage Motion and Path Planning

The large majority of strategies for Coverage Path Planning rely on decomposing the area into cells that must be visited and covered. The whole area is divided using exact or approximate cellular decomposition. Authors in [3][26] adopt grid-based technique to divide the area into squared cells. Each square contains occupancy information of the part of the environment that it covers. Cells are usually explored by back-and-forth motions using single drone such as in [56][62]. Authors in [59][61][68] use multiple drones, and back-and-forth motion to cover the area in offline mode. They aim for less number of turning maneuvers. Other approaches adopt spiral or circular motions. Authors in [54] adopt Spiral motion and use single drone. They aim to cover an area in offline mode in less mission completion-time and shorter distance. Others adopt multiples drones to reduce the path length [57][58]. Authors in [60] relied on Integer Linear Programming for collision avoidance. They try to reduce the flight time and energy consumption. Table I shows a list of CPP related works with the adopted area shape, number of drones, plan status and challenges they tackle.

 ISBN: 978-1-61208-744-3

TABLE I. COVERAGE PATH PLANNING APPROACHES

Ref.	*Area Shape*	*Status*	*Drones*	*Technique/Motion*	*Challenge*
[52]	Circle	NA	Multiple	3D deployment	Increase download link with less power
[53]	Circle	NA	Single	Spiral decomposition	Shorter plans, less runtime
[54]	Irregular	NA	Single	Combine multi data rate scheme	Tracking mobile objects (e.g. bicycles)
[3]	Irregular	Offline	Single	Grid-Based	Minimum completion-time
[26]	Irregular	Offline	Single	Grid-Based	Obtain images to build area map
[55]	Polygonal	Offline	Single	Energy-aware Spiral	Energy consumption
[56]	Polygonal	Offline	Single	Back-and-Forth	reduce turning maneuvers, Path length
[57][58]	Polygonal	Offline	Multiple	Spiral	Path length
[59]	Polygonal	Offline	Multiple	Back-and-Forth	Number of turning maneuvers
[60]	Rectangular	NA	Multiple	Mixed Integer Linear Programming	Flight time
[61]	Rectangular	Offline	Multiple	Back-and-Forth (Line Formation)	Target detection, Search time, # of UAVs and info. exchange
[62]	Rectangular	NA	Single	Back-and-Forth, Square	Fixed and mobile target detection, Coverage rate
[63]	Square	NA	Multiple	Multi objective	Minimum cost, lowest altitude possible
[28]	Graph Grid	Online	Multiple	Edge Counting and Patrol-GRAPH*	Path length; Robots distance average
[64]	Rectangular	Online	Multiple	Reinforced Random Walk	Coverage time; Global detection efficiency

III. Contribution

In this work, we are going to use one rotary wing drone to cover an area in an offline mode without obstacles and non-flying zones. We planned the path using Grid based technique with tractor mobility path pattern. We applied sub-division on the main heatmap to tune the path and reduce the number of turns and save energy. The main phases in our path planning method are presented below:

A. Cellular decomposition

- *Generate Grid-cells*: We consider having an image of the Area of Interest in binary format (black/white image). We generate a matrix representation (heatmap) of the area (Figure 1(a)) and map it to a grid-based form (Figure 1(b)). The required matrix dimensions (i.e, length and width) are given by the path planner. It depends on the UAV footprint and determines the size of each grid cell in our work.

  Concerning the scan direction, we choose it to be parallel to the longest side of the grid (length or width). Using principal axis transformation, the longest side of the area is aligned parallel to the Y-axis of the image. Each value on the heatmap represents a percentage of the area covered in a grid cell.

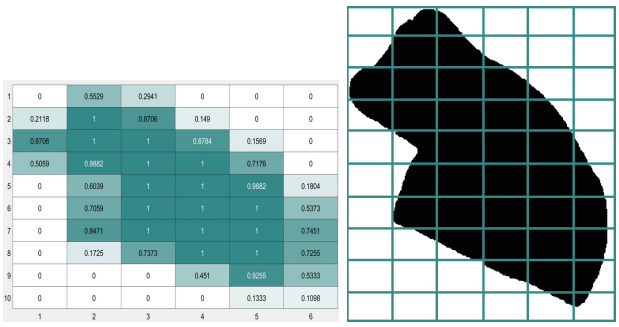

(a) *Heatmap format* (b) *Area mapped to a grid*

Figure 1. Binary image representation using Heatmap of the matrix

- *UAV coverage range*: The path planer defines the coverage range for the UAV. Basically, a UAV's coverage projection (or footprint) is circular shape. However, due to the usage of grid-based method in our work (i.e, grid-cells have rectangular shape), we consider the rectangle inscribed in the footprint circle (see Figure 2). Each rectangle is going to represent a grid-cell entity.

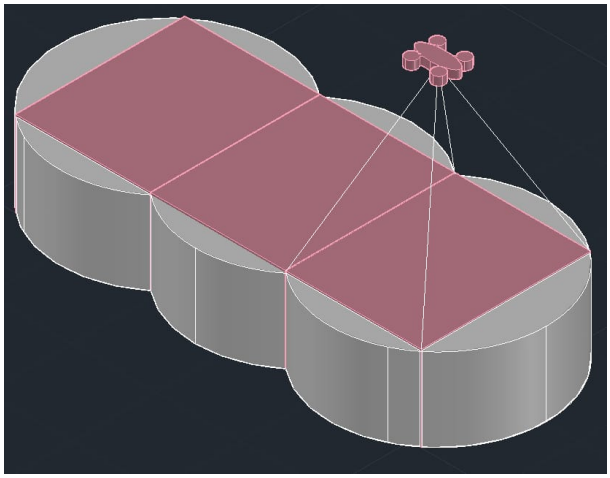

Figure 2. UAV footprint

B. Path Pattern and trajectory generation

1) Basic approach

A tractor mobility pattern covers all nodes without leaving any gap [69]. It pursues parallel tracks to the grid dimensions, as shown in Figure 3(a). The turn angle is always 90°. However, the path crossing points v_1, v_2, v_3 passes through unneeded cell (example cell A1). Since point v_3 is higher than v_1, a UAV has to move to point v_2 and make the rectangular angle.

In our basic plotting approach, we modify the turn angles to get trapezoidal tracks (see Figure 3(b)). By this modification, the path length is shorter. The track's end-point is the center of the last non-zero value cell on the track. A path track crosses the center of the grid cells that have non-zero values.

For example, in Figure 3(b), assume that the UAV is positioned at v_1 and is moving upward. Instead of moving to cell A1, a turn is to be done at point v_2 (cell A2) which

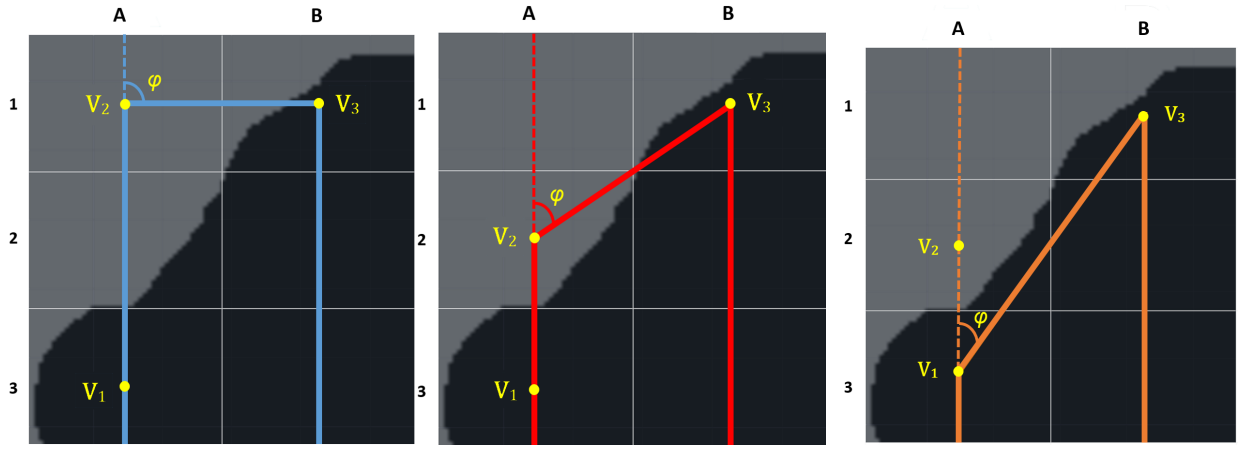

(a) *Rectangular Turn-angle 90°* (b) Modified turn angle (c) Modified Turning Position (Basic approach)

Figure 3. Tractor mobility- Trapezoidal and Rectangular Turns

is the center of the last non-zero-value cell. The calculation of the turn angle is explained in section III-B3.

Another concern can be raised when the grid cell contains small portion of the area. Is it possible to cover the portion without moving to the center of the grid as this avoids long path? In Figure 3(b), cell A2, a small portion of the area exists. the same portion of the area can be covered by moving directly from v_1 to v_3 as shown in Figure 3(c). This can reduce the energy consumed during the movement. The below section explains how we plan the new trajectory. The main ideas discussed below are (a) the selection of the turning positions, (b) the selection of the start point and the direction of the trajectory.

2) Path turning and plotting points

In order to determine the accurate position at which a turning is to be done, we divide each grid cell into a group of 4 subcells. The new heatmap of the area in Figure 1(a) is presented in Figure 4.

1	0	0	0	0.5647	0.2275	0	0	0	0	0	0	0
2	0	0	0.651	1	0.8314	0	0	0	0	0	0	0
3	0	0.1373	0.9686	1	1	0.5333	0	0	0	0	0	0
4	0	0.6118	1	1	1	0.9882	0.4706	0	0	0	0	0
5	0.6118	1	1	1	1	1	1	0.6157	0	0	0	0
6	0.9059	1	1	1	1	1	1	1	0.5255	0	0	0
7	0.4902	1	1	1	1	1	1	1	0.9843	0.2392	0	0
8	0	0.5098	1	1	1	1	1	1	1	0.7176	0	0
9	0	0	0.4196	0.9686	1	1	1	1	1	0.9843	0.2039	0
10	0	0	0.05882	0.9059	1	1	1	1	1	1	0.549	0
11	0	0	0.3412	1	1	1	1	1	1	1	0.8863	0.06275
12	0	0	0.5804	1	1	1	1	1	1	1	1	0.302
13	0	0	0.8235	1	1	1	1	1	1	1	1	0.4627
14	0	0	0.7647	1	1	1	1	1	1	1	1	0.5137
15	0	0	0	0.498	0.9725	1	1	1	1	1	1	0.5098
16	0	0	0	0	0.2588	0.8314	1	1	1	1	1	0.4157
17	0	0	0	0	0	0.06275	0.5882	0.9882	1	1	1	0.2471
18	0	0	0	0	0	0	0	0.2275	0.7176	1	0.9098	0.0549
19	0	0	0	0	0	0	0	0	0	0.4667	0.5216	0
20	0	0	0	0	0	0	0	0	0	0	0	0
	1	2	3	4	5	6	7	8	9	10	11	12

Figure 4. Resulted Heat-Map after the subdivision (grid: 20 x12)

Figure 5(b) represents the heatmap of Figure 3(c) after subdivision. We investigate the heatmap values of the subcells to determine at which side the portion of the area is located in the cell, as well as, the turning position and degree.

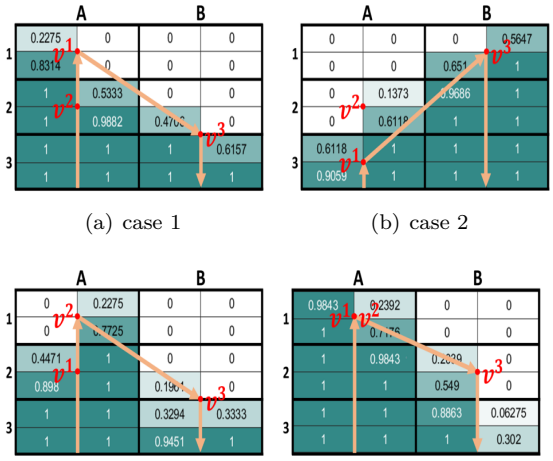

(a) case 1 (b) case 2

(c) case 3 (d) case 4

Figure 5. Subdivision of a grid cell

The main steps in the trajectory generation are:

- **Step 1:** Perform the subdivision of the original grid cells and generate the new heatmap. Assume the original dimensions are L x W, the new grid dimensions are $L' = max\{2W, 2L\}$ and $W' = min\{2W, 2L\}$. We denote by $\mathscr{H}$ the matrix as follows:

$$\mathscr{H} = \{h_{ij} \in [0,1] | i \in [1, L'] \wedge j \in [1, W']\}$$

  Each grid cell has a positive value in the heatmap $\mathscr{H}$.
- **Step 2:** We denote by ζ the set of non-zero columns in the grid ($|\zeta| <= W'$). A column p (denoted ζ_p) belongs to ζ if and only if the following holds:

$$\zeta_p \in \zeta \Leftrightarrow \exists h_{ip} > 0 \wedge i \in [1, L']$$
$$\zeta_p = \{h_{ij} \in \mathscr{H} | j = p \wedge i \in [1, L']\}$$

  thus,

$$\zeta = \{\zeta_p | p \in [1, W']\}$$

Let F_p denotes the first non-zero cells in column ζ_p (see Figure 6):

$$F_p = \{h_{ip} \in \zeta_p | h_{ip} > 0 \wedge i < i', \forall i' \in [1, L']\}$$

Let L_p denote the Last non-zero cells in column ζ_p as follows:

$$L_p = \{h_{ip} \in \zeta_p | h_{ip} > 0 \wedge i > i', \forall i' \in [1, L']\}$$

The cardinalities of F_p and L_p are $|F_p| = |L_p| = 1$. For example, in Figure 4, ζ_3 has F_3 located at row 2 and L_3 located at row 14.

We start the trajectory planning from the first column in ζ. Each path track (denoted q) is going to be the vertical middle line between two adjacent columns in the grid. Track q_1 is the vertical middle line between ζ_1 and ζ_2, Track q_2 is the middle line between ζ_3 and ζ_4 and so on. We are going to

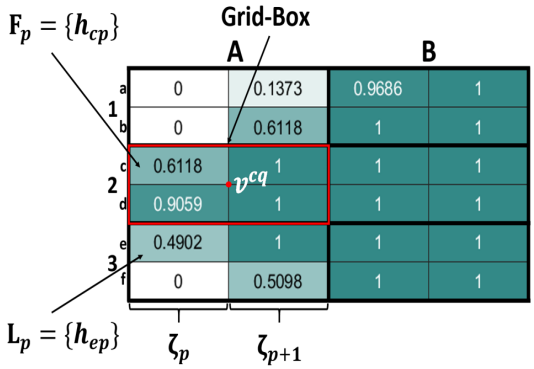

Figure 6. Notations

investigate the positions of F_p and L_p in order to determine the turning points of each track. It should be noted that the two points of a track segment are the track start-point and turning-point. Except for the last track that has only a start-point and a stop-point.

- **Step 3:** Formally, a grid is represented as graph $G(V, E)$, where V is the set of nodes and E is the set of edges. The center of the grid box (or range) formed by 4 adjacent cells represents a node v in the graph (see Figure (6)). These nodes (once determined) will be linked together to form the final path.

  In general, for two columns ζ_p and ζ_{p+1}, the range at row r and row (r+1), is denoted

  $$[h_{rp}: h_{(r+1)(p+1)}]$$

  , where r$\in [1, L'[$. Let v^{rq} be the center of this range.

  Two cases occurs (see Figure 7):

  (1) If the end-point of a track q is located from the side of the first elements of ζ_p and ζ_{p+1}, the two possible turning points (or nodes) are:

  - The center of the range that contains the first element in ζ_p.
  - The center of the range that contains the first element in ζ_{p+1}.

  (2) If the end-point of a track q is located from the side of the last elements of ζ_p and ζ_{p+1}, the ranges for the turning points are calculated from the Last elements of ζ_p and ζ_{p+1}. In this case, the two points are:

  - The center of the range that contains the Last element in ζ_p.
  - The center of the range that contains the Last element in ζ_{p+1}.

  The range is the same as defined above.

  If $h_{(r+1)(p+1)} = 0$ or $h_{(r+1)p} = 0$ or $r = L'$, the range becomes:

  $$[h_{(r-1)p} : h_{r(p+1)}]$$

- **Step 4:** To tune the path and choose between the two possible turning points on a track q, we follow the steps presented in Figure 8. Assume that the start direction of track q is vertical ascending, the algorithm indicates the turning point as well as, the next node on the coming track (q+1). This point is the start point of the new track. The algorithm checks the position of each node in the grid in order to draw the path link from one track to another. This link forms an edge of the graph.
- **Step 5:** According to our trajectory pattern, for each track, there are two options for the direction:

  Option1: UAV moves vertically ascending from the side of last element (L_p) of the track q to the first element (F_p). In this case, a turning point is located on the side of the First element. The corresponding path planning was described in the previous sections.

  Option2: UAV moves vertically descending from the side of the first element of the track p (F_p) to the last element (L_p). In this case, the turning point of track q and the start point of track (q+1) are located on the side of the last element. The same steps described in the previous presented algorithm (Figure 8) are applied. We reverse the operators in the conditions.

  3) Turn angle calculation

  Let's go back to Figure 3(c), the turn angle at point v_2 is the exterior angle between nodes v_1, v_2, v_3. We denote it φ_{123}.

  Each node $v \in V$ has coordinate (x, y) in the cartesian plan. Let v_i, $v_j \in V$ denote specific nodes and $e_{ij} \in E$ denotes an edge between nodes v_i and v_j. $d(v_i, v_j)$ is the distance between them.

$$d(v_i, v_j) = \sqrt{\left(x_{v_i} - x_{v_j}\right)^2 + \left(y_{v_i} - y_{v_j}\right)^2} \quad (1)$$

The turn angle at point v_j can be calculated from the internal angle $\angle v_i v_j v_k$ as follows:

$$\varphi_{ijk} = \pi - \cos^{-1}(\angle v_i v_j v_k) \quad (2)$$

where $\cos^{-1}(\angle v_i v_j v_k)$ is found using the law of cosines in the triangle $\triangle v_i v_j v_k$. Consequently,

 ISBN: 978-1-61208-744-3

Algorithm 1

Input: $\zeta_p \wedge \zeta_{p+1}$
Output: Two possible turning points on a track q
{**If end-point of q is from the side of** F_p **&** F_{p+1} }
Find F_p for ζ_p
$r_1 \leftarrow$ row of F_p
Find F_{p+1} for ζ_{p+1}
$r_2 \leftarrow$ row of F_{p+1}
{1^{st} possible turning point}
$v^{r_2q} \leftarrow$ center of grid box $[h_{r_2p} : h_{(r_2+1)(p+1)}]$
{2^{nd} possible turning point}
$v^{r_1q} \leftarrow$ center of grid box $[h_{r_1p}: h_{(r_1+1)(p+1)}]$
{**If end-point of q is from the side of** L_p **&** L_{p+1} }
Find L_p for ζ_p
$r_1 \leftarrow$ row of L_p
Find L_{p+1} for ζ_{p+1}
$r_2 \leftarrow$ row of L_{p+1}
{1^{st} possible turning point}
if $(r_1 == L')$ **then**
  $v^{r_1q} \leftarrow$ center of grid box $[h_{(r_1-1)p} : h_{r_1(p+1)}]$
else
  if $(h_{(r_1+1)(p+1)} == 0)$ **then**
    $v^{r_1q} \leftarrow$ center of grid box $[h_{(r_1-1)p} : h_{r_1(p+1)}]$
  else
    $v^{r_1q} \leftarrow$ center of grid box $[h_{r_1p}: h_{(r_1+1)(p+1)}]$
  end if
end if
{2^{nd} possible turning point}
if $(r_2 == L')$ **then**
  $v^{r_2q} \leftarrow$ center of grid box $[h_{(r_2-1)p} : h_{r_2(p+1)}]$
else
  if $(h_{(r_2+1)p} == 0)$ **then**
    $v^{r_2q} \leftarrow$ center of grid box $[h_{(r_2-1)p} : h_{r_2(p+1)}]$
  else
    $v^{r_2q} \leftarrow$ center of grid box $[h_{r_2p}: h_{(r_2+1)(p+1)}]$
  end if
end if

Figure 7. Algorithm 1 generates two possible turning points

$$\varphi_{ijk} = \pi - \cos^{-1}\left[\frac{(d(v_i,v_j)^2 + d(v_j,v_k)^2 - d(v_k,v_i)^2)}{2d(v_i,v_j)d(v_j,v_k)}\right] \quad (3)$$

It has been mentioned earlier that UAV's power consumption decreases when the number of turns performed during the mission decreases [67]. We aim to have a compromise between the length of the generated path and the number of turn in such a way to cover the whole area with minimum energy consumption and completion-time. We took different scenarios to evaluate the time and energy consumption. The results are shown in Section IV.

Algorithm 2

Input: $v^{r_1q} \wedge v^{r_2q} \wedge \zeta$
Output: The turning point on track q and the start point on track (q+1)
$r_3 \leftarrow$ row of F_{p+2}
$v^{r_3(q+1)} \leftarrow$ center of grid box $[h_{(r_3)(p+2)} : h_{(r_3+1)(p+3)}]$
{for simplification}
$v_1 \leftarrow v^{r_1q}$
$v_2 \leftarrow v^{r_2q}$
$v_3 \leftarrow v^{r_3(q+1)}$
{Below Case refers to Figure 5(a)}
if $(r_1 > r_2)$ **then**
  The turning point $\leftarrow v_1$
  Move from v_1 to v_3
end if
{Below Case refers to Figure 5(b)}
if $(r_1 < r_2) \wedge (r_2 < r_3)$ **then**
  The turning point $\leftarrow v_1$
  Move from v_1 to v_3
end if
{Below Case refers to Figure 5(c)}
if $(r_1 < r_2) \wedge (r_2 >= r_3)$ **then**
  The turning point $\leftarrow v_2$
  Move from v_2 to v_3
end if
{Below Case refers to Figure 5(d)}
if $(r_1 == r_2)$ **then**
  The turning point $\leftarrow v_1$
  Move from v_1 to v_3
end if

Figure 8. Tuning the trajectory from track q to track q+1

IV. Computational Experiments and Result

In this section, we perform a set of comparisons with different flight patterns. We demonstrate the performance of our proposed method for the CPP problem.

The performance metrics are completion-time and energy consumption.

- *Completion-Time:* We adopt the formula [3] below to compute the completion-time:

$$T = \frac{S}{V} + \sum_{u=1}^{k} \frac{\varphi_u}{\omega} \quad (4)$$

where completion-time is denoted by T, S for route length, V is UAV movement speed, while k is the number of turns, φ is the angle of u^{th} turn and ω is the UAV rotation rate.

- *Energy model:* We adopt the following energy model [67] to evaluate our work. Below we give a quick recapit-

 ISBN: 978-1-61208-744-3

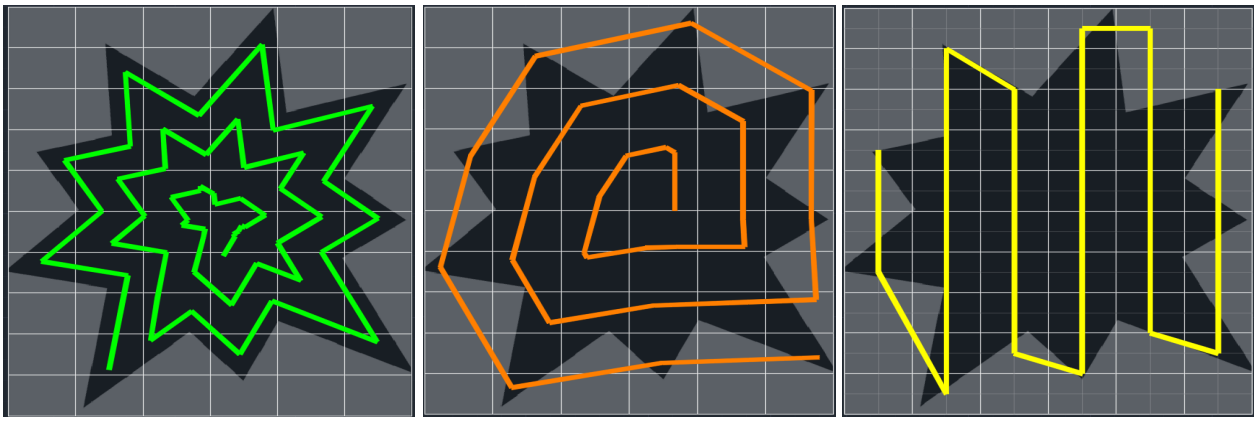

(a) *Trajectory by Basic Spiral motion* (b) Trajectory by Spiral convex hull (c) Trajectory by our work

Figure 9. Trajectory planning in Spiral motion v/s our work

ulation on the model components. Let $c(e_{ij})$ denotes the energy cost of traversing the edge e_{ij} between these nodes.

$$c(e_{ij}) = \lambda d(v_i, v_j) \tag{5}$$

where λ denotes the energy consumption per unit length. It is related to the UAV characteristics.

Let $c(\varphi_u)$ be the cost associated with a feasible turn. It is proportional to the angle of the turn φ_u.

$$c(\varphi_u) = \gamma \frac{180}{\pi} \varphi \tag{6}$$

The total energy E consumed is the sum of two terms. The first term is proportional to the distance traveled and the second term is proportional to the sum of turn angles.

$$\mathrm{E} = \sum_{i \in \mathrm{V}} \sum_{j \in \mathrm{V}} c(e_{ij}) + \sum_{i \in \mathrm{V}} \sum_{j \in \mathrm{V}} \sum_{k \in \mathrm{V}} c(\varphi_{ijk}) \tag{7}$$

In our experimentation, we assume that $\lambda = 0.1164$ KJ/unit length and $\gamma = 0.0173$ KJ/degree.

(i) Scenario 1: We compared our algorithm to the basic spiral and spiral convex hull patterns on irregular star area shape. The grid is 10rows*6columns. The grid cell dimension is (0.98274 x 1.39335 $unit^2$). The paths are presented in Figure 9.

We assume that the UAV speed = 0.5 unit/sec and UAV rotation rate ω= 30 degree/sec. The paths are compared according to completion-time and energy consumption. The comparative results are presented in Table II. The table shows that our path length is 15.499% shorter than the spiral path pattern in Figure 9(a). It is also 6.666% shorter than the path in Figure 9(b) with reduction of 81.725% and 15.01% in number of turns in degree. This means our approach achieves better energy saving. Results show that the mission completion-time is reduced by 54.27% by our work over Figure 9(a) and by 8.76% over Figure 9(b), with energy saving of 76.85% and 12.92% compared to Figure 9(a) and Figure 9(b) respectively. In

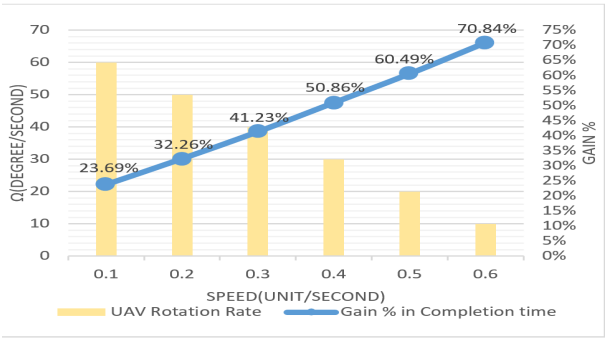

Figure 10. Gain in completion-time in our work compared to Spiral path in Figure 9(a)

TABLE II. SPIRAL MOTIONS V/S OUR WORK

	Spiral Figure 9(a)	***Spiral Figure 9(b)***	***Our work***
Route length S in units	58.1238	52.6216	49.1151
UAV speed V in unit/sec	0.5	0.5	0.5
Number of Turns k	48	27	24
Turns in degree	4925	1059	900
Rotation rate ω in degree/sec	30	30	30
Completion-time T in sec	280.4143	140.5432	128.2302
Energy consumption E in KJ	91.97282	24.44687	21.28786

Figure 10, we present the gain percentage in completion-time in our work over the results of Figure 9(a). We take different UAV speed and rotation rate values. Results show mission time reduction up to 70.84%.

In Figure 11, we present the gain percentage in completion-time in our work over the results of Figure 9(b). We take different UAV speed and rotation rate values. Results show mission time reduction up to 11.23%.

- **More irregular shapes:** We explore the performance of our algorithm on other irregular shapes. In

TABLE III. ENERGY CONSUMPTION AND MISSION COMPLETION-TIME COMPARED TO SPIRAL TECHNIQUE

Shapes	*Path Length (unit)*		*Sum of Angles (degree)*		*Completion-time* (sec.)		*Energy consumed (KJ)*		*Energy Saving*
	(a)	*(b)*	*(a)*	*(b)*	*(a)*	*(b)*	*(a)*	*(b)*	
L Shape (Figure 12)	160	187.3	450	540	350	404.6	34.2	37.4	8.55%
U Shape (Figure 13)	200	209.8	540	540	430	449.6	38.8	40	3%
Y Shape (Figure 14)	130	158.2	540	540	290	346.4	30.7	34	9.7%

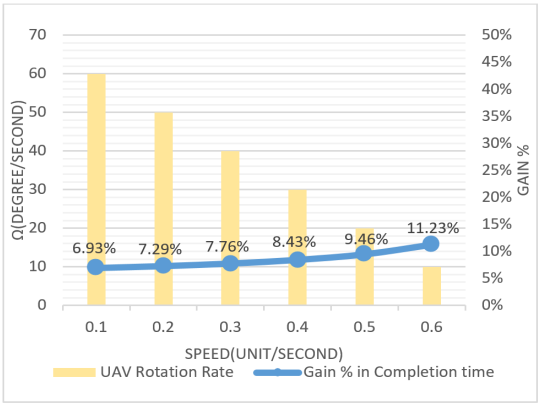

Figure 11. Gain in completion-time in our work compared to Spiral convex hull in Figure 9(b)

this section, we compare our work to other irregular shapes (L, U, Y shapes).

Figure 12, Figure 13 and Figure 14 show the trajectory planning in L shape, U shape and Y shape area respectively. The comparison is between our approach and Spiral technique. The scenarios are tested with a speed v=0.5 $unit/sec$ and a rotation degree ω= 30 $degree/sec$ assuming that the grid cell dimension is 10*10 $unit^2$.

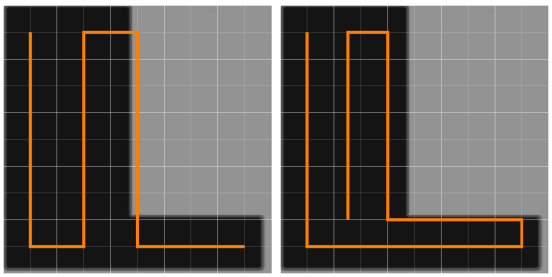

(a) Trajectory by our work(b) *Trajectory by Basic Spiral motion*

Figure 12. L Shape - Trajectory planning

The performance of our algorithm is presented in Table III. The table shows the energy consumed and completion-time while covering the different area shapes. Our algorithm performs between 3% and 9% energy saving over spiral technique.

(ii) Scenario 2: We compared our method to trajectory

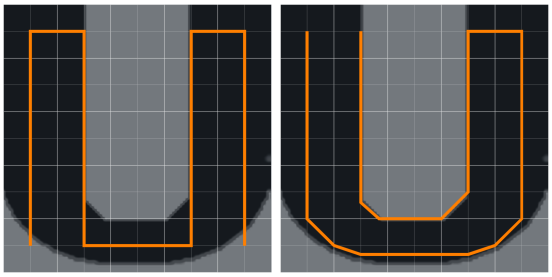

(a) Trajectory by our work (b) Trajectory by Basic Spiral motion

Figure 13. U Shape - Trajectory planning

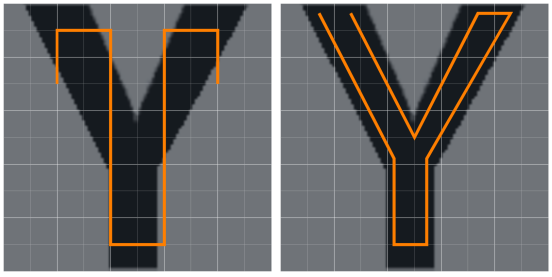

(a) Trajectory by our work (b) Trajectory by Basic Spiral motion

Figure 14. Y Shape - Trajectory planning

plan proposed in [3]. The grid dimensions are 10 rows x 6 columns. The path patterns are shown in Figure 15, where the cell dimension is (0.9894 x 1.3934 $unit^2$). The values are shown in Table IV. We assume that the UAV speed = 0.5 unit/sec and UAV rotation rate ω= 30 degree/sec.

TABLE IV. RESULTS OBTAINED BY THE TRAJECTORY PLAN IN in FIGURE 15(a) AND FIGURE 15(b)

	(a) Ref.[3]	*(b) Our work*
Route length S in units	50.2747	41.2304
UAV speed V in unit/sec	0.5	0.5
Number of Turns k	17	10
Total Turns in degree	1530	900
Rotation rate ω in degree/sec	30	30
Completion-time T in sec	151.5494	112.4608
Energy consumption E in KJ	32.32034	20.36884484

 ISBN: 978-1-61208-744-3

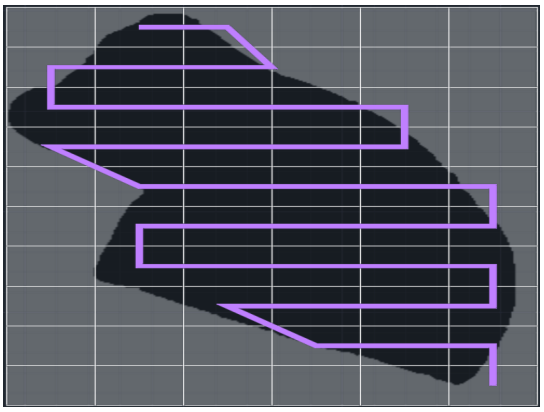

(a) Trajectory plan by the work done in Ref. [3]

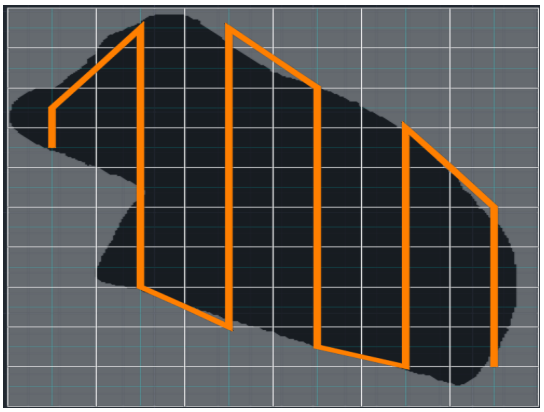

(b) Trajectory plan by our work

Figure 15. Trajectory planning in our work v/s CPP's algorithm in Ref. [3]

Table IV shows that our path is 17.989% shorter than the path in Figure 15(a) with reduction of 41.17% in number of turns. This means better energy saving. Results show that the mission completion-time is reduced by 25.79% in our work, with energy saving of 36.98% compared to the results obtained in [3]. It should be noted that the area is not totally covered by the work in [3]. There are two cells in Figure 15(a) that are part of the area and the drone didn't cover them. However, in our work all required cells are covered.

In Figure 16, we present the gain percentage in completion-time in our work over the work in [3]. We take different UAV speed and rotation rate values. Results show mission time reduction up to 32.97%.

(iii) Scenario 3: We compared our trajectory plan to work presented in [26] on an area grid of dimension 6rowsx10columns. The obtained path patterns are presented in Figure 17. The cell dimension is 1 x 1 $unit^2$. The resulted values are shown in Table V.

Table V shows that our path is 8.301% shorter than the path in [26] with reduction in number of turns by 61.904%. As for the completion-time, it is reduced by 29.37% in our work, with a 53.53% less in energy consumption.

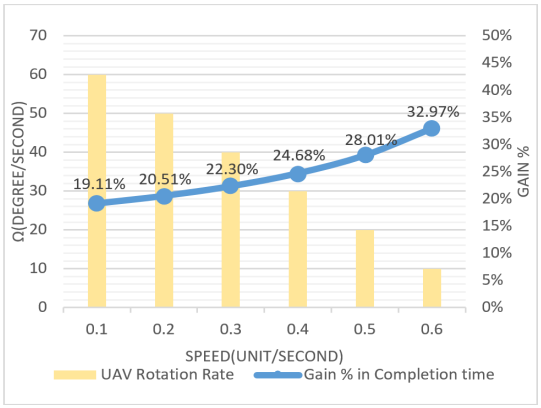

Figure 16. Gain in completion-time in our work compared to Ref. [3]

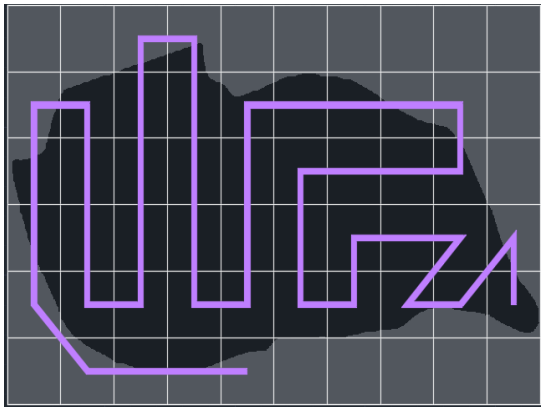

(a) Trajectory plan by the work done in Ref. [26]

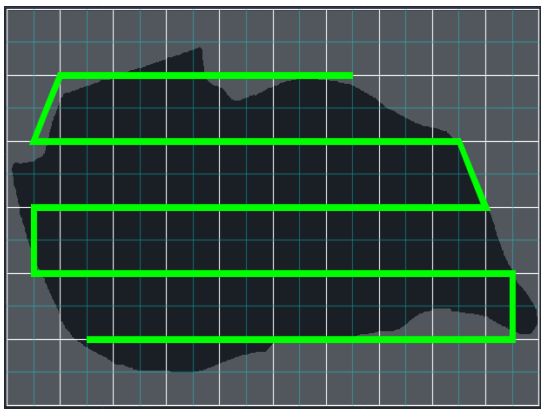

(b) Trajectory plan by our work

Figure 17. Trajectories obtained by the CPP in Ref. [26] and our CPP method

In Figure 18, we present the gain in completion-time in our work over the work in [26]. We take different speed values and rotation rates. Results show a gain up to 45.82% in time reduction in our work.

TABLE V. RESULTS OBTAINED BY THE PLAN IN FIGURE 17(a) AND FIGURE 17(b)

	(a)Ref.[26]	*(b)Our work*
Route length S in unit length	48.6268	44.5875
UAV speed V in unit/sec	0.5	0.5
Number of Turns k	21	8
Total Turns in degree	1890	720
Rotation rate ω in degree/sec	30	30
Completion-time T in sec	160.2536	113.175
Energy consumption E in KJ	36.22407	16.833379

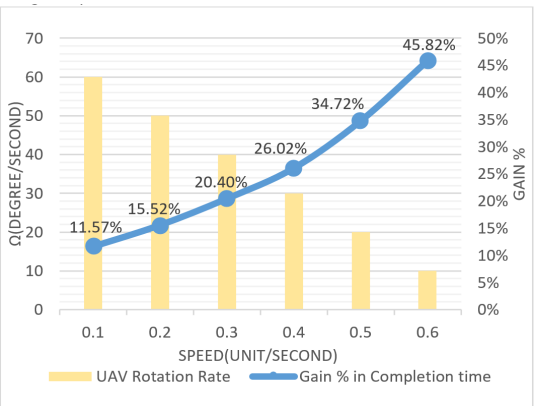

Figure 18. Reduction in completion-time in our work over the work in Ref. [26]

V. Conclusion

We proposed an energy aware coverage path planning method. In our work, we use one drone to cover areas without obstacles and nonflying zones in an offline mode. The results show that our work covers the whole area and has lower completion-time and energy consumption in comparison to the state of the art and the test cases used. In the future work, we plan to extend the proposed method to study the CPP in the presence of obstacles in the Area of Interest.

References

[1] N. Basilico and S. Carpin, "Deploying teams of heterogeneous uavs in cooperative two-level surveillance missions," in *2015 IEEE/RSJ International Conference on Intelligent Robots and Systems (IROS)*, Sep. 2015, pp. 610–615.

[2] P. Lottes *et al.*, "Uav-based crop and weed classification for smart farming," in *2017 IEEE International Conference on Robotics and Automation (ICRA)*, May 2017, pp. 3024–3031.

[3] L. H. Nam, L. Huang, X. J. Li, and J. F. Xu, "An approach for coverage path planning for uavs," in *2016 IEEE 14th International Workshop on Advanced Motion Control (AMC)*, April 2016, pp. 411–416.

[4] L. Chunbo *et al.*, "Unmanned aerial vehicles for disaster management," in *Springer*, 08 2019, pp. 83–107.

[5] A. Hansen, "Applying visitor monitoring methods in coastal and marine areas – some learnings and critical reflections from sweden," *Scandinavian Journal of Hospitality and Tourism*, pp. 1–18, 03 2016.

[6] K. Park and R. Ewing, "The usability of unmanned aerial vehicles (uavs) for measuring park-based physical activity," *Landscape and Urban Planning*, vol. 167, pp. 157–164, 11 2017.

[7] D. Leary, "Drones on ice: an assessment of the legal implications of the use of unmanned aerial vehicles in scientific research and by the tourist industry in antarctica," *Polar Record*, vol. 53, pp. 1–15, 05 2017.

[8] H. X. Pham, H. M. La, D. Feil-Seifer, and M. Deans, "A distributed control framework for a team of unmanned aerial vehicles for dynamic wildfire tracking," in *2017 IEEE/RSJ International Conference on Intelligent Robots and Systems (IROS)*, Sep. 2017, pp. 6648–6653.

[9] L.-P. Chrétien, J. Théau, and P. Menard, "Visible and thermal infrared remote sensing for the detection of white-tailed deer using an unmanned aerial system," *Wildlife Society Bulletin*, vol. 40, pp. 181–191, 02 2016.

[10] S. Wich, D. Dellatore, M. Houghton, R. Ardi, and L. Koh, "A preliminary assessment of using conservation drones for sumatran orang-utan (pongo abelii) distribution and density," *Journal of Unmanned Vehicle Systems*, vol. 4, pp. 45–52, 11 2015.

[11] D. Stark, I. P. Vaughan, L. Evans, H. Kler, and B. Goossens, "Combining drones and satellite tracking as an effective tool for informing policy change in riparian habitats: A proboscis monkey case study," *Remote Sensing in Ecology and Conservation*, pp. 44–52, 07 2017.

[12] W. Ken *et al.*, "Remote sensing of the environment with small unmanned aircraft systems (uass), part 2: Scientific and commercial applications," *Journal of Unmanned Vehicle Systems*, vol. 2, pp. 86–102, 09 2014.

[13] P. Vihervaara *et al.*, "How essential biodiversity variables and remote sensing can help national biodiversity monitoring," *Global Ecology and Conservation*, vol. 10, pp. 43 – 59, 2017.

[14] J. Jiménez López and M. Mulero-Pázmány, "Drones for conservation in protected areas: Present and future," *Drones*, vol. 3, no. 1, 2019. [Online]. Available: https://www.mdpi.com/2504-446X/3/1/10

[15] I. Petkovic, D. Petkovic, and r. Petkovics, *IoT Devices vs. Drones for Data Collection in Agriculture*, 01 2017, pp. 063–080.

[16] A. Fotouhi, H. Qiang, M. Ding, M. Hassan, L. G. Giordano, A. García-Rodríguez, and J. Yuan, "Survey on UAV cellular communications: Practical aspects, standardization advancements, regulation, and security challenges," *CoRR*, vol. abs/1809.01752, 2018. [Online]. Available: http://arxiv.org/abs/1809.01752

[17] E. Grøtli and T. Johansen, "Path planning for uavs under communication constraints using splat! and milp," *Journal of Intelligent and Robotic Systems*, vol. 65, pp. 265–282, 08 2012.

[18] C. Di Franco and G. Buttazzo, "Coverage path planning for uavs photogrammetry with energy and resolution constraints," *Journal of Intelligent & Robotic Systems*, vol. 83, pp. 445–462, 02 2016.

[19] PwC, "global report on the commercial applications of drone technology," https://www.pwc.pl/pl/pdf/clarity-from-above-pwc.pdf, 09 2017.

[20] M. Khan, B. A. Alvi, E. Safi, and I. Khan, "Drones for good in smart cities:a review," *International Conference on Electrical, Electronics, Computers, Communication, Mechanical and Computing (EECCMC)*, 01 2018.

[21] J. C. Rosser, V. Vignesh, B. A. Terwilliger, and B. C. Parker, "Surgical and medical applications of drones: A comprehensive review." *JSLS Journal of the Society of Laparoendoscopic Surgeons*, vol. 22, no. 3, p. e2018.00018, 2018.

[22] N. R. Zema, E. Natalizio, M. Poss, G. Ruggeri, and

A. Molinaro, "MeDrone: On the use of a medical drone to heal a sensor network infected by a malicious epidemic," *Ad Hoc Networks*, vol. 50, pp. 115–127, Nov. 2016. [Online]. Available: https://hal.archives-ouvertes.fr/hal-01396858

[23] F. Mohammed, A. Idries, N. Mohamed, J. AlJaroodi, and I. Jawhar, "Uavs for smart cities: Opportunities and challenges," *International Conference on Unmanned Aircraft Systems (ICUAS)*, pp. 267–273, 05 2014.

[24] N. R. Zema, E. Natalizio, and E. Yanmaz, "An Unmanned Aerial Vehicle Network for Sport Event Filming with Communication Constraints," in *BalkanCom 2017 First International Balkan Conference on Communications and Networking*, Tirana, Albania, May 2017. [Online]. Available: https://hal.archives-ouvertes.fr/hal-01731379

[25] O. Artemenko, O. J. Dominic, O. Andryeyev, and A. Mitschele-Thiel, "Energy-aware trajectory planning for the localization of mobile devices using an unmanned aerial vehicle," in *2016 25th International Conference on Computer Communication and Networks (ICCCN)*, Aug 2016, pp. 1–9.

[26] J. Valente, D. Sanz, J. Cerro, A. Barrientos, and M. de Frutos, "Near-optimal coverage trajectories for image mosaicing using a mini quad-rotor over irregular-shaped fields," *Precision Agriculture*, vol. 14, pp. 115–132,, 02 2013.

[27] D. Li, X. Wang, and T. Sun, "Energy-optimal coverage path planning on topographic map for environment survey with unmanned aerial vehicles," *Electronics Letters*, vol. 52, no. 9, pp. 699–701, 2016.

[28] C. Recchiuto, C. Nattero, A. Sgorbissa, and R. Zaccaria, "Coverage algorithms for search and rescue with uav drones - abstract," in *In Workshop of the XIII AIIA Symposium on Artificial Intelligence*, 12 2014.

[29] C.-M. Tseng, C.-K. Chau, K. Elbassioni, and M. Khonji, "Flight tour planning with recharging optimization for battery-operated autonomous drones," 03 2017. [Online]. Available: https://arxiv.org/abs/1703.10049

[30] C. Di Franco and G. C. Buttazzo, in *Energy-aware Coverage Path Planning of UAVs*, 04 2015, pp. 111–117.

[31] J. Ware and N. Roy, in *An analysis of wind field estimation and exploitation for quadrotor flight in the urban canopy layer*, 05 2016, pp. 1507–1514.

[32] W. Al-Sabban, L. Gonzalez, and R. Smith, "Wind-energy based path planning for electric unmanned aerial vehicles using markov decision processes," in *Proceedings of the IEEE/RSJ International Conference on Intelligent Robots and Systems. IEEE*, 01 2013.

[33] M. Coombes, W.-H. Chen, and C. Liu, in *Boustrophedon coverage path planning for UAV aerial surveys in wind*, 06 2017, pp. 1563–1571.

[34] J. Gross, S. Goetz, and J. Cihlar, "Application of remote sensing to parks and protected area monitoring: Introduction to the special issue," *Remote Sensing of Environment*, vol. 113, pp. 1343–1345, 07 2009.

[35] C. Imen *et al.*, "Design and performance analysis of global path planning techniques for autonomous mobile robots in grid environments," *International Journal of Advanced Robotic Systems*, vol. 14, 04 2017.

[36] H. Xu, L. Shu, and M. Huang, "Planning paths with fewer turns on grid maps," in *Proceedings of the Sixth International Symposium on Combinatorial Search*, 2013, pp. 193–201.

[37] J. Gubbi, R. Buyya, S. Marusic, and M. Palaniswami, "Internet of things (iot): A vision, architectural elements, and future directions." *Future Generation Comp. Syst.*, vol. 29, no. 7, pp. 1645–1660, 2013. [Online]. Available: http://dblp.uni-trier.de/db/journals/fgcs/fgcs29.htmlGubbiBMP13

[38] P. Simoens, M. Dragone, and S. A., "The internet of robotic things: A review of concept, added value and applications." *International journal of Advanced Robotic Systems*, vol. 15, no. 1, p. 1729881418759424, 2018. [Online]. Available: https://doi.org/10.1177/1729881418759424

[39] S. Chandrasekharan *et al.*, "Designing and implementing future aerial communication networks," *IEEE Communications Magazine*, vol. 54, no. 5, pp. 26–34, May 2016.

[40] H. Choset, "Coverage for robotics–a survey of recent results," *Annals of mathematics and artificial intelligence*, vol. 31, no. 1-4, pp. 113–126, 2001.

[41] S. Bochkarev, S.and Smith, "On minimizing turns in robot coverage path planning." in *Proceedings of the 2016 IEEE International Conference on Automation Science and Engineering (CASE)*, August 2016, p. 18–20.

[42] E. Galceran and M. Carreras, "A survey on coverage path planning for robotics," *Robotics and Autonomous systems*, vol. 61, no. 12, pp. 1258–1276, 2013.

[43] A. Majeed and S. Lee, "A new coverage flight path planning algorithm based on footprint sweep fitting for unmanned aerial vehicle navigation in urban environments," *Applied Sciences (Switzerland)*, vol. 9, 04 2019.

[44] S. Nasr, H. Mekki, and K. Bouallegue, "A multi-scroll chaotic system for a higher coverage path planning of a mobile robot using flatness controller," *Chaos Solitons Fractals*, vol. 118, p. 366–375, 2019.

[45] K. Zhou *et al.*, "Agricultural operations planning in fields with multiple obstacle areas," *Computers and Electronics in Agriculture*, vol. 109, pp. 12–22, 2014.

[46] A. Montanari, F. Kringberg, A. Valentini, C. Mascolo, and A. Prorok, "Surveying areas in developing regions through context aware drone mobility," in *Proceedings of the 4th ACM Workshop on Micro Aerial Vehicle Networks, Systems, and Applications*, ser. DroNet'18. New York, NY, USA: ACM, 2018, pp. 27–32. [Online]. Available: http://doi.acm.org/10.1145/3213526.3213532

[47] F. Lingelbach, "Path planning using probabilistic cell decomposition." in *Proceedings of the 2004 IEEE International Conference on Robotics and Automation, ICRA'04*, vol. 1, 2004, p. 467–472.

[48] H. Choset, "Coverage of known spaces: The boustrophedon cellular decomposition." *Autonomous Robots*, vol. 9, p. 247–253, 2000.

[49] H. Choset *et al.*, "Principles of robot motion: Theory, algorithms, and implementation," *MIT Press*, 2005.

[50] S. Wong, "Qualitative topological coverage of unknown environments by mobile robots," *Doctoral Dissertation, The University of Auckland, New Zealand*, 2006.

[51] V. Shivashankar *et al.*, "Real-time planning for covering an initially-unknown spatial environment," in *Proceedings of the Twenty-Fourth International Florida Artificial Intelligence Research Society Conference*, May 2011, p. 18–20.

[52] R. Díaz-Delgado, G. Ónodi, G. Kröel-Dulay, and M. Kertész, "Enhancement of ecological field experimental research by means of uav multispectral sensing," *Drones*, vol. 3, no. 1, p. 7, 2019.

[53] M. Mozaffari, W. Saad, M. Bennis, and M. Debbah, "Efficient deployment of multiple unmanned aerial vehicles for optimal wireless coverage," *IEEE Communications Letters*, vol. 20, 06 2016.

[54] W. Yue and Z. Jiang, "Path planning for uav to collect sensors data based on spiral decomposition," *Procedia Computer Science*, vol. 131, pp. 873–879, 01 2018.

 ISBN: 978-1-61208-744-3

[55] T. M. Cabreira, C. D. Franco, P. R. Ferreira, and G. C. Buttazzo, "Energy-aware spiral coverage path planning for uav photogrammetric applications," *IEEE Robotics and Automation Letters*, vol. 3, no. 4, pp. 3662–3668, Oct 2018.

[56] M. Torres, D. A. Pelta, J. L. Verdegay, and J. C. Torres, "Coverage path planning with unmanned aerial vehicles for 3d terrain reconstruction," *Expert Systems with Applications*, vol. 55, pp. 441–451, 2016.

[57] F. Balampanis, I. Maza, and A. Ollero, in *Area decomposition, partition and coverage with multiple remotely piloted aircraft systems operating in coastal regions*, 07 2016, pp. 275–283.

[58] Balampanis, Fotios and Maza, Ivan and Ollero, Anibal, "Area partition for coastal regions with multiple uas," *Journal of Intelligent and Robotic Systems*, vol. 88, no. 2, pp. 751–766, Dec 2017. [Online]. Available: https://doi.org/10.1007/s10846-017-0559-9

[59] J. Fortuna, S. P.B, and J. Sousa, in *Multiple UAV area decomposition and coverage*, 04 2013, pp. 30–37.

[60] E. J. Forsmo, E. Grøtli, T. Fossen, and T. Johansen, in *Optimal search mission with Unmanned Aerial Vehicles using Mixed Integer Linear Programming*, 05 2013, pp. 253–259.

[61] J. Acevedo, B. Arrue, I. Maza, and A. Ollero, "Distributed approach for coverage and patrolling missions with a team of heterogeneous aerial robots under communication constraints," *International Journal of Advanced Robotic Systems*, vol. 10, pp. 1–13, 01 2013.

[62] H. L. Andersen, "Path planning for search and rescue mission using multicopters," 2014.

[63] C. Caillouet and T. Razafindralambo, in *Efficient deployment of connected unmanned aerial vehicles for optimal target coverage*, 10 2017, pp. 1–8.

[64] D. Albani, D. Nardi, and V. Trianni, in *2017 IEEE/RSJ International Conference on Intelligent Robots and Systems (IROS)*, Sep. 2017, pp. 4319–4325.

[65] J. J. Acevedo, B. C. Arrue, I. Maza, and A. Ollero, "Cooperative large area surveillance with a team of aerial mobile robots for long endurance missions," *Journal of Intelligent & Robotic Systems*, vol. 70, no. 1, pp. 329–345, Apr 2013. [Online]. Available: https://doi.org/10.1007/s10846-012-9716-3

[66] C. Wenkai *et al.*, "Development of a power line inspection robot with hybrid operation modes*," in *2017 IEEE/RSJ International Conference on Intelligent Robots and Systems*, 09 2017, p. 973–978.

[67] J. Modares, F. Ghanei, N. Mastronarde, and K. Dantu, in *UB-ANC planner: Energy efficient coverage path planning with multiple drones*, 05 2017, pp. 6182–6189.

[68] G. Öst, "Search path generation with uav applications using approximate convex decomposition," Master's thesis, Linköping UniversityLinköping University, Automatic Control, The Institute of Technology, 2012.

[69] S. Rashed and M. Soyturk, "Analyzing the effects of uav mobility patterns on data collection in wireless sensor networks," *Sensors*, vol. 17, 02 2017.

 ISBN: 978-1-61208-744-3